Effective two-body model for spectra of clusters of ^{2}H, ^{3}H, ^{3}He, and ^{4}He with ^{4}He, and ^{2}H-^{4}He scattering

P. R. Fraser,[1,*] K. Massen-Hane,[1] A. S. Kadyrov,[1] K. Amos,[2,3] I. Bray,[1] and L. Canton[4]
[1]*Department of Physics, Astronomy and Medical Radiation Sciences, Curtin University, GPO Box U1987, Perth 6845, Australia*
[2]*School of Physics, University of Melbourne, Victoria 3010, Australia*
[3]*Department of Physics, University of Johannesburg, P.O. Box 524, Auckland Park 2006, South Africa*
[4]*Istituto Nazionale di Fisica Nucleare, Sezione di Padova, I-35131 Padova, Italy*
(Received 5 January 2017; revised manuscript received 3 July 2017; published 28 July 2017)

Four light-mass nuclei are considered by an effective two-body clusterization method: ^{7}Li as ^{3}H + ^{4}He, ^{7}Be as ^{3}He + ^{4}He, ^{8}Be as ^{4}He + ^{4}He, and ^{6}Li as ^{2}H + ^{4}He. The low-energy spectra of the first three are determined from single-channel Lippmann-Schwinger equations. For the last, two uncoupled sets of equations are considered: those involving the $^3S_1$ and those of the posited $^1S_0$ states of ^{2}H. Low-energy elastic scattering cross sections are calculated from the same ^{2}H + ^{4}He Hamiltonian, for many angles and energies for which data are available. While some of these systems may be more fully described by many-body theories, this work establishes that a large amount of data may be explained by these two-body clusterizations.

DOI: 10.1103/PhysRevC.96.014619

I. INTRODUCTION

The scattering and cluster spectra formed by an α particle with each of the four light-mass nuclei considered herein constitute basic information required for studies of nuclear reactions responsible for the relative abundances of light atomic nuclei observed throughout the universe. These arose from the big bang, and in light stars ($\leqslant 1.5 M_\odot$) proton-proton chain reactions lead to the formation of nuclei up to mass 8. Once the α particles generated in those reactions are present in sufficient number, the triple-α process can produce ^{12}C, the crucial feature being the energy of the Hoyle state in ^{12}C lying just above the breakup threshold. In the triple-α process, the first two α particles fuse to form ^{8}Be whose instability to α decay results in an equilibrium concentration of ^{8}Be in stellar environments.

As noted by Dubovichenko and Uzikov [1], experimental studies of astrophysical nuclear reaction properties are complicated by the fact that the energies of most relevance are extremely low; frequently so low that direct measurement is nearly impossible. Thus, astrophysical quantities are often extrapolated from scattering data taken at higher energies, and such linear extrapolation is not always justified. In addition, experimental errors in measured cross sections are often large (for radiative capture cross sections they are as much as 100 percent), depreciating the results of any extrapolation. In such cases, theoretical predictions such as those presented herein can be necessary.

In recent years, the spectra and elastic scattering of these light mass cluster systems has become of interest as test beds for modern theoretical techniques. For example, Refs. [2–4] used the resonating group method with the no-core shell model (RGM-NCSM) and Ref. [5] used an Alt-Grassberger-Sandhas three-body approach to that end. An interesting method of analytic continuation of the elastic scattering data at positive energies to negative energies was investigated in Ref. [6], and applied to extract bound-state properties of the ^{2}H + ^{4}He system.

Dubovichenko and Uzikov [1] note that while there are many microscopic models of the continua of light mass nuclei, they usually entail cumbersome multichannel calculations, the accuracy of which cannot always be determined reliably. Consequently, with the view toward current or future assessments of astrophysical aspects of nuclear physics, the application of relatively simple, but realistic, models is justified. Usually such model calculations are set by finding the best agreement with available low-energy scattering data. Herein we follow that procedure but add the requirement that the cluster model reproduce the low lying spectrum (bound and resonant) of the compound nucleus, including the binding energy relative to the cluster pair threshold.

In this way we consider the light mass clusters leading to the four compound nuclei of interest to be describable with an effective two-body, single-channel model. None of the four nuclei forming the clusters have low-lying excited states below nucleon breakup thresholds. However the compound systems formed, ^{6}Li, ^{7}Li, ^{7}Be, and ^{8}Be, do. We use a Sturmian expansion approach to solve Lippmann-Schwinger (LS) equations; an approach that provides a low energy spectrum (bound and continuum states) of the compound nucleus formed by each cluster considered, as well as giving the relevant S matrices with which scattering cross sections can be evaluated.

In this investigation, we calculate the low-energy elastic scattering cross section of the ^{4}He + ^{2}H system and the low-energy spectrum of ^{6}Li from the same clusterization, both using the same interaction potential. Investigation of the low-energy scattering of deuterons from ^{4}He dates back to experimental work in the 1930s [7]. As noted, Refs. [2–4] used a RGM-NCSM method and considered ^{2}H-^{4}He scattering, among other reactions. Reference [5] used an Alt-Grassberger-Sandhas three-body method in momentum space at deuteron energies of 4.81 and 17.0 MeV also for the ^{2}H-^{4}He system.

*paul.fraser@curtin.edu.au

 ©2017 American Physical Society

While details of this scattering may be investigated in a more fundamental way, e.g., by using three- or six-body approaches, it remains useful to investigate how much of the spectrum and cross section may be explained by a simpler two-body clusterization. A similar phenomenological semimicroscopic model has been used recently to calculate phase shifts, for which a good match to data was obtained [1] as was the calculated S factor for capture.

We have also used the same method to specify the spectra of ^{7}Li and ^{7,8}Be from the clusters of ^{3}H, ^{3}He, and ^{4}He with ^{4}He respectively. Spectra of ^{7}Li and ^{7}Be have been found previously [8] by solving the coupled-channel problems of nucleons coupling to ^{6}He and ^{7}Be nuclei allowing for the nucleons to interact with low excitation states of the nuclei. The results agreed well with known states in the spectra. Here we do not have a coupled-channel problem since, for the range of energies we consider, all nuclei involved can be taken to be in their ground states. The spectra of the two mass-7 nuclei have two bound states and two resonance states below ∼7 MeV excitation.

The last system we consider, ^{8}Be, has only two resonance states in its low excitation spectrum: the ground and first excited states at 3.03 MeV. The next resonance state has a centroid of 11.35 MeV. The ground state resonance lies just 0.0918 MeV above the two-α breakup threshold and is very narrow (5.57 eV); both features are crucially important in the three-α stellar process. The ^{4}He-^{4}He cluster calculation is of the simplest form in the effective two-body approach, and the two resonance states can be found with appropriate energy values.

In the next section we give a précis of the method used and follow that with a short statement on the forms of charge distributions used to ascertain the Coulomb interactions of the clusters. Then in Sec. IV we report on the spectra of the clusters ^{7}Li and ^{7,8}Be found with the method we have used. The spectra and scattering cross sections for the ^{2}H-^{4}He cluster are then given and discussed in Sec. V. Conclusions are drawn in Sec.VI.

II. STURMIAN EXPANSION SOLUTIONS OF LIPPMANN-SCHWINGER EQUATIONS

The method uses separable expansions of the assumed interaction potentials between two nuclei. The form factors in that expansion are derived from Sturmian functions defined from the chosen two-cluster interaction potentials. In the cases of ^{4}He coupled with ^{3}H, ^{3}He, and another ^{4}He cluster, the two nuclei have no excited states of low excitation. For example ^{4}He has resonance states, but they lie above 20 MeV excitation. Thus, we deal with single channel interactions of a spin-$\frac{1}{2}$ or spin-0 particle with a spin-0 ^{4}He. With the ^{2}H-^{4}He clusterization, we consider that there are two uncoupled sets of equations to solve; those formed by the $^{3}S_1$ and, separately, the $^{1}S_0$ states of the ^{2}H.

Then with channels $c = (l, I)$; J^{π} (l is the orbital quantum number of relative motion, I the spin 0, $\frac{1}{2}$, or 1 as appropriate for the nucleus chosen to cluster with an ^{4}He nucleus), the LS equations for the single-channel T matrices have the form

$$T^{J^{\pi}}_{cc'}(p,q;E) = V^{J^{\pi}}_{cc'}(p,q) + \mu \sum_{c''} \int_0^{\infty} V^{J^{\pi}}_{cc''}(p,x) \times \frac{x^2}{k^2 - x^2 + i\epsilon} T^{J^{\pi}}_{c''c'}(x,q;E)dx, \quad (1)$$

where the momentum $k = \sqrt{\mu E}$, with μ designating $2m_{\rm red}/\hbar^2$; $m_{\rm red}$ is the reduced mass. Solutions of Eq. (1) are sought using the (finite sum) expansion

$$V_{cc'}(p,q) \sim \sum_{n=1}^{N} \hat{\chi}_{cn}(p)\, \eta_n^{-1} \hat{\chi}_{c'n}(q). \quad (2)$$

To evaluate scattering cross sections, one needs the S matrices which are linked to the T matrices as [9,10]

$$\begin{aligned} S_{cc'} &= \delta_{cc'} - i\pi\mu k_{c'} T_{cc'} \\ &= \delta_{cc'} - i^{(l_{c'} - l_c + 1)} \pi\mu \sum_{n,n'=1}^{N} \sqrt{k_c}\hat{\chi}_{cn}(k_c) \\ &\quad \times ([\boldsymbol{\eta} - \mathbf{G}_0]^{-1})_{nn'} \hat{\chi}_{c'n'}(k_{c'})\sqrt{k_{c'}}, \end{aligned} \quad (3)$$

In this representation, $\mathbf{G_0}$ and η have matrix elements

$$\begin{aligned} [\mathbf{G}_0]_{nn'} &= \mu \sum_c \int_0^{\infty} \hat{\chi}_{cn}(x) \frac{x^2}{k^2 - x^2 + i\epsilon} \hat{\chi}_{cn'}(x)dx, \\ [\boldsymbol{\eta}\,]_{nn'} &= \eta_n \delta_{nn'}. \end{aligned} \quad (4)$$

Bound states of the compound system, if they exist, are defined by the zeros of the matrix determinant in Eq. (3) when the energy, E, is less than zero.

The input matrices of potentials are taken to have the form

$$\begin{aligned} V_{cc'}(r) = V^{\rm coul}_{cc'}(r) + [V_0 \delta_{c'c} f(r) + V_{\ell\ell} f(r)\, [\ell \cdot \ell] \\ + V_{II} f(r)[\mathbf{I} \cdot \mathbf{I}] + V_{\ell I} g(r)[\ell \cdot \mathbf{I}]]_{cc'}, \end{aligned} \quad (5)$$

wherein local form factors (Woods-Saxon functions)

$$f(r) = \left[1 + e^{\left(\frac{r-R}{a}\right)}\right]^{-1}, \quad g(r) = \frac{1}{r}\frac{df(r)}{dr}, \quad (6)$$

are used. If needed, the surface can be deformed ($R = R(\theta\phi) = R_0[1 + \epsilon]$). Details of this and of the relevant matrix elements are given in Ref. [11]. $V^{\rm coul}_{cc'}(r)$ are elements of the Coulomb potential matrix. The forms we use are given in the next section.

III. CHARGE DISTRIBUTIONS FOR THE NUCLEI AND THE COULOMB INTERACTION BETWEEN THEM

We assume both nuclei in the cluster have finite charge distributions of three parameter Fermi (3pF) form, *viz.*,

$$\rho_{\rm ch}(r) = \rho_0 \left[1 + w_c \left(\frac{r}{R_c}\right)^2\right] \frac{1}{1 + \exp\left(\frac{r - R_c}{a_c}\right)}, \quad (7)$$

where R_c and a_c are the radius and diffuseness parameters for a Woods-Saxon distribution, and w_c is a scaling parameter. The central charge density is that with which the volume integral of the distribution equates to the charge of the nucleus represented.

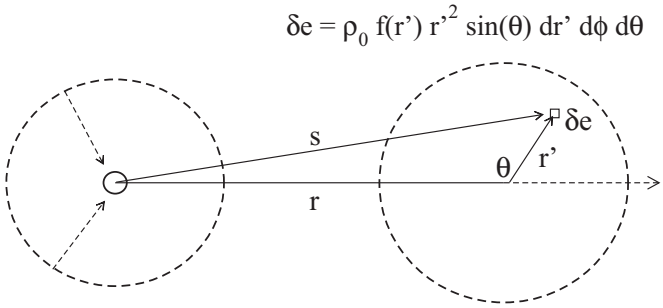

FIG. 1. The geometry for two interacting nuclei, both having a 3pF charge distribution.

To define the Coulomb interaction between such charge distributions, first consider that felt by a positively charged point test particle with charge δe and a general spherical charge distribution, $\rho_0 f(r)$, i.e.,

$$V_{\rm coul}^{(pt)}(r) = \delta e \int \rho_0 f(r') \frac{1}{|\mathbf{r}' - \mathbf{r}|} d\mathbf{r}'. \quad (8)$$

After expanding in multipoles and performing angular integration, the only nonzero component comes from the s wave ($\ell = 0$), whence

$$V_{\rm coul}^{(pt)}(r) = 4\pi(\delta e)\rho_0 \int_0^\infty f(r') v_{\ell=0}(r',r) r'^2 dr'. \quad (9)$$

where $v_{\ell=0}(r',r) = \frac{1}{r_>}$ with $r_>$ and $r_<$ being the greater and lesser of r' and r, respectively. The radial integration splits into two terms, giving

$$V_{\rm coul}^{(pt)}(r) = 4\pi(\delta e)\rho_0 \left[\frac{1}{r} \int_0^r f(s) s^2 ds + \int_r^\infty \frac{1}{s} f(s) s^2 \, ds \right]. \quad (10)$$

With both nuclei in the clusterization having 3pF charge distributions, the field given in Eq. (10) is folded with the 3pF charge distribution for the second body. The geometry is as shown in Fig. 1.

With $s = \sqrt{r^2 + r'^2 - 2rr'\cos(\theta)}$, the Coulomb potential is

$$V_{\rm coul}(r) = 2\pi \int_0^\infty r'^2 f(r') dr' \int_0^\pi V_{\rm coul}^{(pt)}(s) \sin(\theta) \, d\theta. \quad (11)$$

For ^{4}He, the parameter values of the 3pF charge distribution are as given in Ref. [12,13]. They are $R_c = 1.008$ fm, $a_c = 0.327$ fm, and $w = 0.445$. As ^{3}H is listed [12,13] as also having a root-mean-square (rms) charge radius of 1.7 fm, the ^{4}He parameter set has been used for its charge distribution as well. ^{3}He is listed [12,13] as having a slightly larger rms charge radius, 1.88 fm. As there is no specified set of 3pF parameters given, we considered a range of values for them, since, as shown in Ref. [14], variation in the three parameters leads to minimal difference in results provided the rms charge radius is kept constant. The set used is listed in Table I.

For ^{2}H, the rms charge radius has been determined [15] to be 2.13 fm. To have that value with the average distribution of the single proton smeared out over an appreciable distance, that rms radius is met using the set of 3pF parameters $R = 0.012$ fm, $a_c = 0.592$ fm, and $w_c = 0$.

TABLE I. Diverse 3pF parameter values giving a root-mean-square charge radius of 1.88 fm.

R_c	1.02	1.02	1.04	1.04	1.06	1.06	1.08	1.08	1.1
a_c	0.358	0.362	0.358	0.362	0.356	0.36	0.356	0.36	0.356
w	0.49	0.43	0.48	0.42	0.5	0.44	0.49	0.46	0.48

IV. STUDIES OF THE ^{3}H + ^{4}He, ^{3}He + ^{4}He AND ^{4}He + ^{4}He SYSTEMS

These cases are taken to be single-channel problems given that the components are quite strongly bound and have no excited states below nucleon emission thresholds. However, the compound systems do have well established spectra and, for the ^{3}H + ^{4}He and ^{3}He + ^{4}He systems, the states that we might expect to obtain with a potential model are those indicated in Table II. The reactions involving ^{4}He that lead to them, or have the mass-7 states as a compound system, are indicated by the check marks.

No orthogonalizing pseudopotential (OPP) [17] to effect inclusion of the Pauli principle has been used in treating these clusters as single-channel problems since all states found thereby are orthogonal. Thus any state that should be blocked because it requires the 7 or 8 nucleons to lie in the 0s shell simply can be ignored. Only if there is channel coupling does a problem arise in ensuring that the Pauli principle is satisfied [11]. With channel coupling, all resultant states of the cluster are linear combinations of all states of the same spin-parity defined in the potentials for each of the target states considered.

A. The ^{3}H + ^{4}He and ^{3}He + ^{4}He systems

Spectra of ^{7}Li and ^{7}Be have been found previously [8] using the multi-channel algebraic scattering (MCAS) program written for spin-$\frac{1}{2}$ particles coupling to a nucleus. The results agreed well with known states in the spectra. A program has now been written for ^{4}He (spin-0) particles coupling to a nucleus. This has been used to again calculate the spectra for the compound nuclei, ^{7}Li and ^{7}Be, as a check against the results found earlier [8].

For the check run, the interaction with strength parameter values (in MeV), $V_0 = -76.8$, $V_{ll} = 1.15$, and $V_{ll} = 2.34$ was used. The geometry of the Woods-Saxon form was set with $R_0 = 2.39$ and $a = 0.68$ fm. The Coulomb potential was set, as in Ref. [8], to be that from a uniformly charged sphere. The charge radius for the ^{4}He + ^{3}H calculation was taken as $R_c = 2.34$ fm, while a slightly larger charge radius (2.39) was used for the ^{3}He + ^{4}He calculation. These values differ (slightly) from those used previously [8] in a study of the same compound systems but taken as ^{3}H and ^{3}He projectiles coupled to an ^{4}He target. The differences are due primarily to our current use of the nuclear masses listed in Ref. [19] rather than the nucleon mass numbers. Using this interaction, we obtained the results listed in Table III and in the columns with the heading "check." The comparison between the results

TABLE II. States in ^{7}Li and of ^{7}Be relevant to this investigation and known reactions [16] involving ^{4}He that populate them.

J^π	^{7}Li			^{7}Be		
	^{3}H(^{4}He,n)	^{4}He(^{3}He,π^+)	^{4}He(^{4}He,p)	^{4}He(^{3}He,γ)	^{4}He(^{3}He,^{3}He),(^{3}He,p)	^{4}He(^{4}He,n)
$\frac{3}{2}^-$	√	√	√	√		√
$\frac{1}{2}^-$		√	√	√		√
$\frac{7}{2}^-$			√		√	
$\frac{5}{2}^-$		√			√	

given in Ref. [8] and by these check runs is sufficiently good that we deem the two codes used to give equivalent results.

Using 3pF distributions for both nuclei in the clusters instead of the uniform sphere approach above, and with adjusted nuclear potential parameter values, the results listed in Table III in the columns specified as "present" were obtained. For these results, the nuclear interaction parameter values were $V_0 = -80.15$ MeV, $V_{\ell\ell} = 1.1$ MeV, and $V_{\ell I} = 3.0$ MeV with a Woods-Saxon geometry, $R_0 = 2.35$ fm and $a_0 = 0.64$ fm. The 3pF parameter set defined above to give an rms charge radius of 1.7 fm was used for both ^{3}H and ^{4}He, while that used for ^{3}He we choose to be the first set in Table I, namely $R_c = 1.02$ fm, $a_c = 0.358$ fm, and $w_c = 0.49$. Using the other sets of parameter values listed in Table I (all of which gave an rms charge radius of 1.88 fm) varied the spectral energies from those listed by no more 25 keV (centroids and widths).

The "present" results agree to within 200 keV (energies and widths). This is encouraging since only the ^{4}He breakup thresholds (2.47 and 1.59 MeV for ^{7}Li and ^{7}Be) lie in the range shown.

B. The ^{4}He + ^{4}He system

We have evaluated the spectrum resulting for the clusters ^{4}He + ^{4}He as another single-channel problem, since the ^{4}He nucleus is strongly bound and has no other bound state in the (low-energy) spectrum. From Ref. [16], we note that the 0_1^+ and 2_1^+ states of ^{8}Be have been found with the ^{4}He(^{4}He,γ) and ^{4}He(^{4}He,^{4}He) reactions. With a (positive-parity) interaction ($V_0 = -47.1$ MeV, $V_{ll} = 0.4$ MeV, $R_0 = 2.1$ fm, and $a_0 = 0.6$ fm) and the Coulomb potential from folding two 3pF distributions, two low-excitation resonance states for ^{8}Be, relative to the cluster threshold, are found. They are the ground state (0^+) resonance having centroid and width energies of 0.092 MeV and 5 eV (cf. experimental values [18] 0.092 MeV and 5.96 eV) and a first excited (2^+) resonance state with centroid and width energies of 3.16 and 1.11 MeV compared with experimental values of 3.03 and 1.51 MeV respectively. With this simple (local Woods-Saxon) single-channel interaction, no 4^+ resonance state is found, at least below 20 MeV excitation.

In this case, the interaction allows a 0s state bound by 20 MeV, which, due to Pauli blocking, is deemed to be spurious and so has been ignored since all resultant states from the single channel problem are orthonormal.

V. RESULTS FOR THE ^{2}H + ^{4}He SYSTEM; CROSS SECTION AND SPECTRUM OF ^{6}Li.

We consider the ^{2}H-^{4}He system as two single-channel problems: one for the $^3S_1$ (ground) state and the other for the posited $^1S_0$ state of the deuteron. We do not consider the states to be coupled by a spin-isospin changing interaction. The deuteron states are both of positive parity and the low excitation spectrum of ^{6}Li only has positive parity states, so the dominant character of the interaction potentials is of positive parity. The results were obtained using $V_0 = -64.775$, $V_{ll} = 0.93$, $V_{lI} = 1.97$, and $V_{II}^+ = -2.0$ (all in MeV) with a geometry of $R_0 = 2.3$ and $a_0 = 0.43$ fm. We also allowed the potential to have a second-order deformation contribution with $\beta_2 = 0.22$. No negative parity interaction has been used, as no such states are known.

^{6}Li has a known low-energy spectrum containing six states: a $1^+;0$ ground state, followed by $3^+;0$, $0^+;1$, $2^+;0$, $2^+;1$ states, and finally a second $1^+;0$ at 5.65 MeV. The next state

TABLE III. Spectra of ^{7}Li and ^{7}Be from a ^{4}He coupled to ^{3}H and ^{3}He respectively. The energies are in MeV while the widths are in keV. The experimental values are those listed in Ref. [18].

J^π	^{7}Li				^{7}Be			
	Exp.	Present	Check	Ref. [8]	Exp.	Present	Check	Ref. [8]
$\frac{3}{2}^-$	Spurious	−31.1	−29.6	−29.4	Spurious	−29.7	−27.8	−28.0
$\frac{1}{2}^-$	Spurious	−29.6	−28.0	−27.8	Spurious	−28.3	−26.3	−26.4
$\frac{3}{2}^-$	−2.47	−2.49	−2.59	−2.47	−1.59	−1.55	−1.53	−1.53
$\frac{1}{2}^-$	−1.99	−1.81	−1.87	−1.75	−1.16	−0.90	−0.85	−0.84
$\frac{7}{2}^-$	2.18(69)	2.23(83)	2.09(80)	2.12(83)	2.98(175)	3.19(180)	3.14(204)	3.07(180)
$\frac{5}{2}^-$	4.13(918)	4.16(717)	4.05(800)	4.12(834)	5.14(1200)	5.15(1040)	5.13(1250)	5.09(1194)

is 17.98 MeV above the ground state. The 3^+ state appears as a clear resonance in the $^2H + ^4He$ cross section, 2.186 MeV above the ground state (or 0.7117 MeV above the scattering threshold, at $E_d = 1.067$ MeV or $E_\alpha = 2.135$ MeV) [20–26]. Also evident is the 2^+_1 resonance 4.31 MeV above the ^6Li ground state (or 2.8375 MeV above the scattering threshold, at $E_d = 4.253$ MeV or $E_\alpha = 8.507$ MeV) [21,27–29]. Present but less pronounced is the 1^+ resonance 5.65 MeV above the ^6Li ground state (or 4.1757 MeV above the scattering threshold at $E_d = 6.264$ MeV or $E_\alpha = 12.527$) [30,31]. It is possible that Ref. [32] shows data for the 0^+ resonance of ^6Li 3.563 MeV above the ground state (or 2.0887 MeV above the scattering threshold at $E_d = 3.133$ MeV or $E_\alpha = 6.266$ MeV), but the data points are sparse. The 2^+_2 state of ^6Li 4.31 MeV above the ground state (or 2.8357 MeV above the scattering threshold) does not appear in data. Data also exist for higher energies [33–38].

Cross sections calculated at fixed scattering angles using the associated S matrices of Eq. (3) angles are compared to measured data in Figs. 2 and 3. The angles at which calculations have been made are shown in each segment of these figures. The data shown in these figures are taken from Ref. [32] (filled circles) at 37.2°, 50.0°, 51.67°, 90.0°, and 120.0°, from Ref. [22] (open circles) at 38.75°, 48.9°, 90.0°, and 125.0°, from Ref. [27] (filled squares) at 51.9°, 90.0°, 125.3°, and 139.1°, from Ref. [30] (open squares) at 50.36°, 87.23°, 120.1°, 137.5°, 163.0°, and 164.5°, from Ref. [22] (upside down triangles) at 38.75°, 48.9°, 90.0°, and 125.0°, from Ref. [20] (filled triangles) at 90.0° and 120.0°, and from Ref. [21] (open triangles) at 90.1°, 125.2°, 140.7°, and 167.7°. They are given in the segments in which they are closest to the calculation angle. All cross sections are in center-of-mass frame, and projectile energies are all in laboratory frame with an α-particle target. While the calculation is defined with a deuterium target, the appropriate change of frames has been performed.

In both Figs. 2 and 3, two calculated resonance features are evident. They coincide with the first excited, isoscalar, 3^+, and the isoscalar 2^+ states of ^{10}Be. In the middle panel of Fig. 2, the locations of the experimentally known and calculated states of ^{10}Be are shown. In Fig. 3, wherein our results are compared with data taken at backward scattering angles, to more clearly see the structures, the plots are fully logarithmic. Again the 3^+ and 2^+ resonances are most evident and the calculated results for energies above ∼5 MeV are too small, not revealing any resonance effect due to formation of the isoscalar 1^+ and of the isovector 2^+ states. Also shown in the bottom panel is a second calculated result taken from Ref. [4]. Their model gives a better description of the data in the 4 to 8 MeV region. More specifically, the shape of the 3^+ resonance is re-created well at most scattering angles, centroids, and widths and with reasonable strengths. The exception is the result for $\theta_{cm} = 125°$ where, while the resonance effect is noted at the correct centroid energy, the magnitude is too low. Off resonance, our calculated results agree by and large with the available low energy data. For the higher energy region, the resonance feature due to formation of the 2^+ state is well re-created at 50° and 164°, and reasonably well at some of the other angles. The nonresonant background calculated at

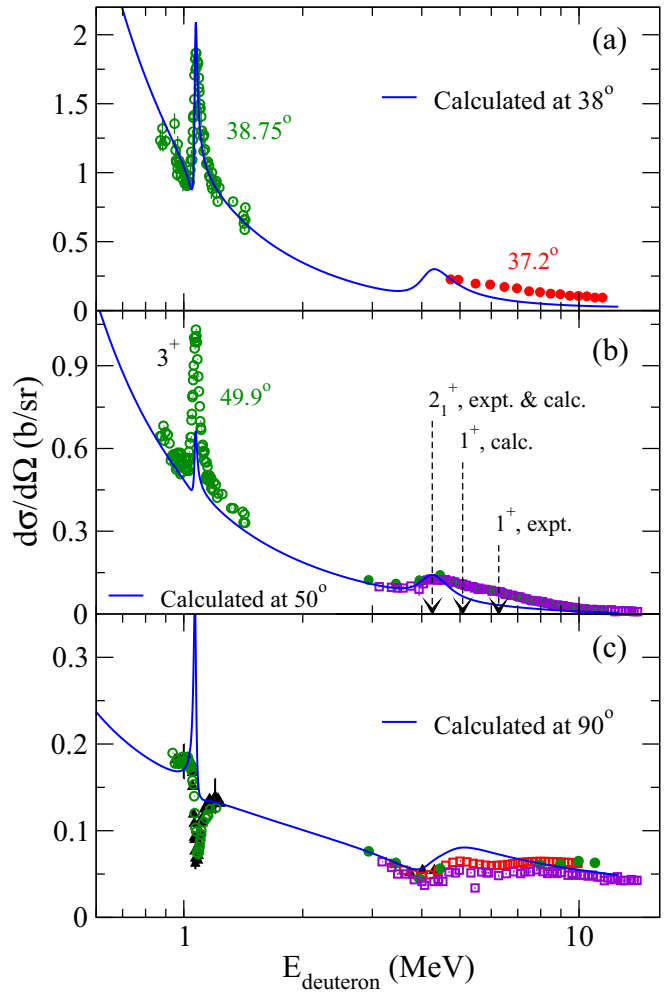

FIG. 2. Experimental elastic cross sections for $^2H + ^4He$ scattering compared with the calculations at fixed angles (a) 38°, (b) 50°, and (c) 90°. The data are from Refs. [20–22,27,30,32]. The 50° panel shows energies where resonances are found in the spectrum, both observed and calculated.

energies above this resonance usually is underestimated and the 1^+ resonance present in the data is not reflected in our calculated results. This resonance was found by the six-body calculation of ^2H-^2He scattering by Ref. [4], however, and so is a distinctive difference in the results of a more sophisticated calculation than ours.

Cross sections calculated at fixed energies are compared to experiment in Figs. 4 and 5. The former shows differential cross sections for eight deuteron energies, ranging from 0.88 to 6.3 MeV. For clarity, the results and data in the left hand panel are depicted semilogarithmically, those in the right hand panel are shown on linear scales. In Fig. 5 we examine five data sets, four of which were also studied in Ref. [4], at 2.935, 6.695, 8.971 and 12 MeV, and the fifth that was studied in Ref. [5]. The notation is as given for Figs. 2 and 3 with additional data depicted as follows: Ref. [39] (filled inverted triangles), Ref. [31] (open inverted triangles), Ref. [40] (left filled triangles), Ref. [41] (open left triangles), and Ref. [42] (filled diamonds).

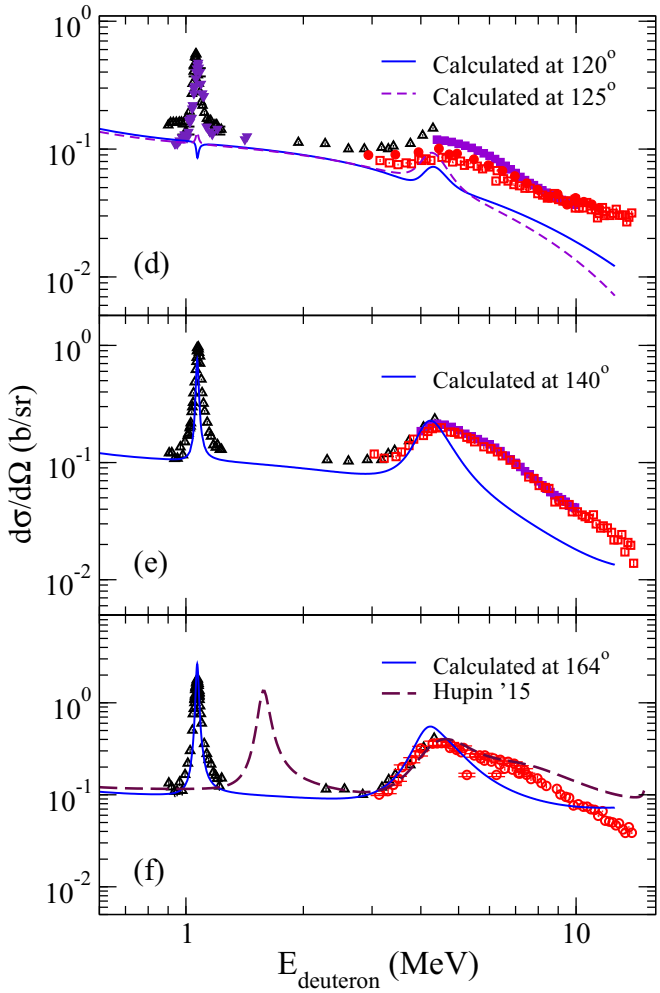

FIG. 3. Experimental elastic cross sections for ^{2}H + ^{4}He compared with the calculations of this work and Ref. [4], at fixed angles (d) 120° and 125°, (e) 140°, and (f) 164°. The data are from Refs. [20–22,27,30,32].

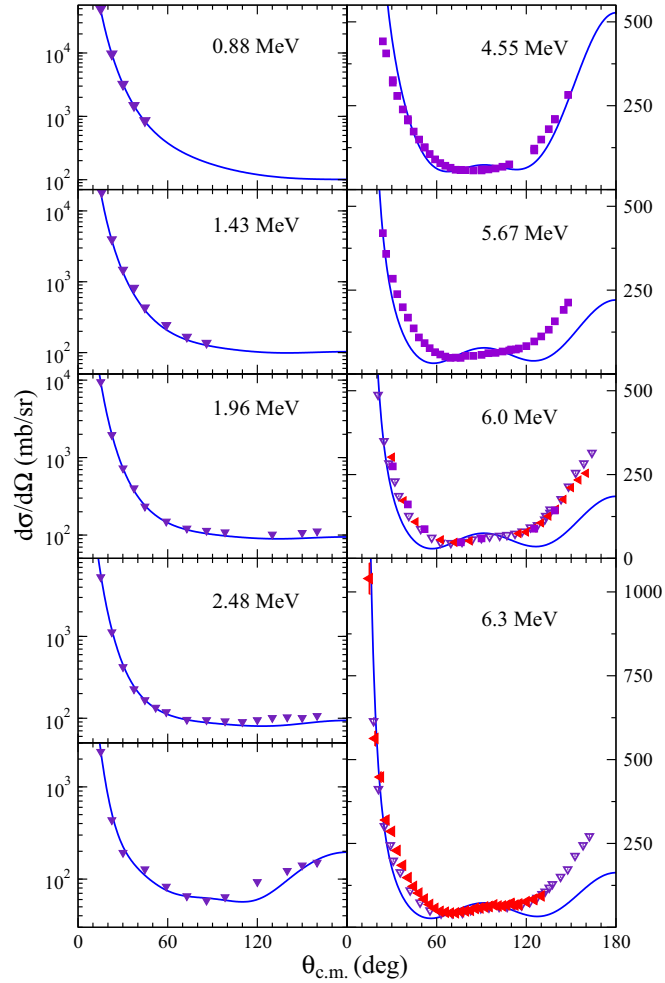

FIG. 4. Experimental elastic cross sections for ^{2}H + ^{4}He scattering, at fixed deuteron energies, compared with the calculations. The data are taken from Refs. [27,31,39,40].

With some exceptions, this two-body calculation tends to reproduce the small-angle scattering better than data at larger angles, matching small-angle data slightly better than the results given in Ref. [4]. However the results found in Ref. [4] are superior to ours at the large scattering angles.

For the lower set of energies, as shown in Fig. 4, our calculated results agree quite well with the data, especially at the four lowest energy values that span the region of the 3^+ resonance. The 4.6 MeV result, near the 2^+ resonance, is quite a good match to data. Above this energy, where the 1^+ resonance is expected to influence results, our results are poorer, as may be expected. In general, at deuteron energies from 4.5 to 6.3 MeV, the calculated cross sections have shapes more pronounced than in the data.

In Fig. 5 we compare a select set of data and our results with the differential cross sections given in Refs. [4,5]. The latter results, shown by the dashed curves, are in excellent agreement with the data at all of the selected energies. Our results are not in as good agreement, but the shapes and magnitudes of them are acceptable in comparison with those revealed in the data.

The same Sturmian approach to solving the Lippmann-Schwinger equations also yields bound-state and resonance energies for the compound nucleus. In Fig. 6 the experimentally known spectrum is compared with that resulting from the calculation. The calculation finds all six known low-energy states of ^{6}Li. Spurious minimal energy states were eliminated when an OPP contribution of $\lambda = 10^6$ MeV was used to block the $1s$ orbit from having more than the four allowed nucleons. They can also simply be discarded, since they are orthogonal to all others.

Owing to the absence of coupling between channel involving the ^{2}H triplet and singlet states, the 0^+_1 and 2^+_1 states are purely found from coupling of the ^{2}H singlet state to the ^{4}He ground state partial waves. All other states are purely found from coupling of the deuteron triplet state to the ^{4}He ground state. The first three excited states are found to within a few tens of eV of data. The final $T = 0$ state, the 1^+_2, is too low in energy by an MeV. The singlet state was assumed to be at the ^{2}H breakup threshold, i.e., 2.224 MeV above the ground state. As there is no mixing between the ^{6}Li $T = 0$ and $T = 1$ states in this calculation, the excitation energies of the two $T = 1$

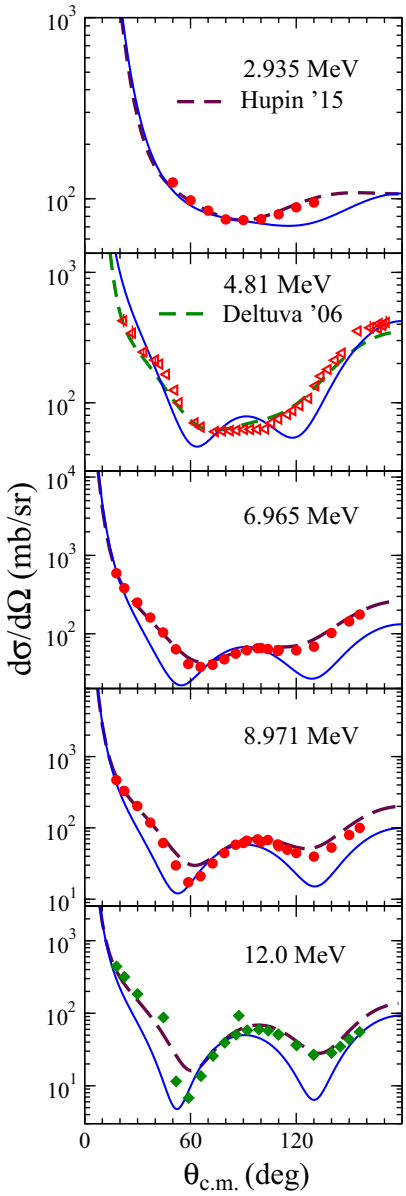

FIG. 5. Experimental elastic cross sections for ^{2}H + ^{4}He scattering, at fixed deuteron energies, compared with calculations of this work and Refs. [4,5]. The data are from Refs. [32,41,42].

states depend linearly on the energy of the ^{2}H singlet state, though the gap between them is set by the interaction potential parameters. This gap is too large by ∼1.1 MeV, and while the energy of the 2^+_2 state is re-created well, the calculated energy of the 0^+ state is too low. It is possible that the antibound singlet state would have a different charge distribution and a different nuclear interaction with the α particle than does the triplet state. However, in this work we opt to use a single interaction, as experimental data are not available to guide selection of the relevant parameters.

While the above approach successfully calculates spectral energies of ^{6}Li, it has limitations with regard to other state properties. The ground state quadrupole moment of ^{6}Li cannot be explained by cluster models such as that used here [43]. At minimum, consideration of tensor correlation is required, and D-wave mixing must be considered in ^{2}H, in ^{4}He, and between these two bodies. Identities in Ref. [44] equate quadrupole deformation with quadrupole moment for collective models such as that used here. Using the measured quadrupole moment, -8.2×10^{-4} [45] yields a deformation $\beta_2 = -0.0313$. This is quite different from the value used herein of $+0.22$, though the comparison is valid only to the extent that the quadrupole deformation of the ^{2}H-^{4}He interaction potential may be equated with the ^{6}Li ground state quadrupole deformation.

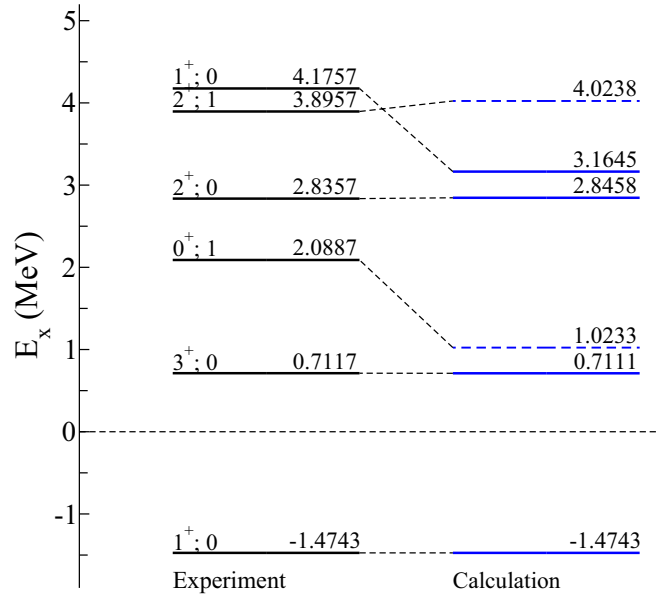

FIG. 6. Experimental spectrum of ^{6}Li compared with the present calculation. In the calculation, solid lines are from coupling to the deuteron $^3S_1$ state, and dashed lines are from coupling to the $^1S_0$ state.

VI. CONCLUSION

The methodology we have used enables all low excitation compound system properties, spin-parities, energies, and widths, extractable from a specific Hamiltonian, to be found. With it, allowance can be made for the effects of the Pauli principle in regards to assumed occupancies of nucleon orbits in the target states. For single-channel problems such as those addressed herein, without such accounting (via orthogonalizing pseudopotentials), spurious states are unique and orthogonal to those that are not. Thus, they can simply be discarded. With the cases studied, all spectral properties are found by solving Lippmann-Schwinger equations. Resonance properties are defined by the poles of the T-matrix associated with the chosen Hamiltonian.

The first cases considered were ^{7}Li and ^{7}Be, formed as the clusters of ^{4}He with ^{3}H and ^{3}He respectively. As the α breakup thresholds are 2.47 and 1.49 MeV respectively, states above those energies were found that are resonances in the cluster evaluations with widths that agree quite well with observation. The widths of resonance states are reaction specific, but as only the ^{4}He breakup channels are relevant in

the energy range considered (the next threshold is 7.25 MeV for neutron emission from ^{7}Li and 5.61 MeV for proton emission from ^{7}Be), those widths then are also the total widths. The good agreement with experimental values is evidence of the model's utility.

The next study made was that of the spectrum for ^{8}Be formed as a cluster of two ^{4}He; a process at the heart of the so-called three α formation of the Hoyle state in ^{12}C in stellar environs. With our two-body approach, we find two low-excitation resonance states in ^{8}Be. They are the ground state (0^{+}) resonance having centroid and width energies of 0.092 MeV and 5 eV (cf. experimental values [18] 0.092 MeV and 5.96 eV) and a first excited (2^{+}) resonance state with centroid and width energies of 3.16 and 1.11 MeV compared with experimental values of 3.03 and 1.51 MeV respectively. Starting with this, we plan full coupled-channel calculations of the $^{4}\mathrm{He} + {}^{8}\mathrm{Be}$ cluster leading to the Hoyle state.

We then considered ^{6}Li as a $^{2}\mathrm{H} + {}^{4}\mathrm{He}$ cluster. We considered the two states of the ^{2}H, the ground $^{3}S_{1}$ and the $^{1}S_{0}$, as uncoupled states and solved two single channel LS equations to obtain estimates of the isoscalar and isovector states in the low-excitation spectrum of ^{6}Li. Four of the possible six states were found to be in good agreement with the known values [18], with only the two highest ones, the 2_{2}^{+} and 1_{1}^{+}, differing by an MeV from the correct energies.

We have also made calculations of $^{2}\mathrm{H} + {}^{4}\mathrm{He}$ scattering at low energies, treating both as single bodies. It was found that this approach re-creates many of the features observed experimentally, though some require a more sophisticated approach. The ^{4}He ground state was coupled to the ^{2}H ground state treated as a pure $^{3}S_{1}$ state, and separately to a $^{1}S_{0}$ resonance, to calculate the spectrum of ^{6}Li. Channels of the $^{3}S_{1}$ and $^{1}S_{0}$ states were not coupled. All six known low-energy ^{6}Li states were re-created, with the first four very close to their known energies and the two most energetic being found at energies that deviate from the measured states by $\sim$1 MeV. The ^{2}H and ^{4}He ground states were coupled to calculate elastic scattering cross sections, and the match to data was overall good. The observed 3^{+} and 2^{+} resonances were re-created, and had the correct shapes and reasonable magnitudes at most angles. The nonresonant cross section was also well reproduced. The observed 1^{+} resonance, however, was not evident in calculated cross sections, though the state is found in the calculated spectrum. Cross sections at fixed angles were good near the two observed resonance energies, though in general results at low angles were a better match to data than those at high angles.

A gauge invariant theory to evaluate capture cross sections using the bound and continuum wave functions derivable from solutions of the Lippmann-Schwinger equations has been developed (and used) for $^{3}\mathrm{H} + {}^{4}\mathrm{He}$ system [46]. Studies of the other cases discussed herein, being important astrophysical quantities, are planned for a future publication.

ACKNOWLEDGMENTS

The authors gratefully acknowledge G. Hupin, S. Quaglioni, P. Navrátil, and A. Deltuva for providing numerical results of their published cross sections. This work is supported by the Australian Research Council and U.S. National Science Foundation under Grant No. PHY-1415656.

[1] S. B. Dubovichenko and Yu. N. Uzikov, Phys. Part. Nucl. **42**, 251 (2011).
[2] S. Quaglioni and P. Navrátil, Phys. Rev. Lett. **101**, 092501 (2008).
[3] P. Navrátil and S. Quaglioni, Phys. Rev. C **83**, 044609 (2011).
[4] G. Hupin, S. Quaglioni, and P. Navrátil, Phys. Rev. Lett. **114**, 212502 (2015).
[5] A. Deltuva, Phys. Rev. C **74**, 064001 (2006).
[6] L. D. Blokhintsev, A. S. Kadyrov, A. M. Mukhamedzhanov, and D. A. Savin, Phys. Rev. C **95**, 044618 (2017).
[7] E. Pollard and H. Margenau, Phys. Rev. **47**, 833 (1935).
[8] L. Canton, G. Pisent, K. Amos, S. Karataglidis, J. P. Svenne, and D. van der Knijff, Phys. Rev. C **74**, 064605 (2006).
[9] G. Cattapan, L. Canton, and G. Pisent, Phys. Rev. C **43**, 1395 (1991), and references cited therein.
[10] G. Pisent and J. P. Svenne, Phys. Rev. C **51**, 3211 (1995).
[11] K. Amos *et al.*, Nucl. Phys. A **728**, 65 (2003).
[12] C. W. de Jager, H. de Vries, and C. de Vries, At. Data. Nucl. Data **14**, 479 (1974).
[13] H. de Vries, C. W. de Jager, and C. de Vries, At. Data. Nucl. Data **36**, 495 (1987).
[14] P. R. Fraser, A. S. Kadyrov, K. Massen-Hane, K. Amos, L. Canton, S. Karataglidis, D. van der Knijff, and I. Bray, J. Phys. G **43**, 095104 (2016).
[15] M. Garçon and J. W. Van Orden, Adv. Nucl. Phys. **26**, 293 (2001).
[16] R. B. Firestone *et al.*, *Table of Isotopes*, 8th ed. (John Wiley & Sons, New York, 1996).
[17] K. Amos, L. Canton, P. R. Fraser *et al.*, Nucl. Phys. A **912**, 7 (2013).
[18] D. R. Tilley *et al.*, Nucl. Phys. A **708**, 3 (2002).
[19] G. Audi, A. H. Wapstra, and C. Thibault, Nucl. Phys. A **729**, 337 (2003).
[20] T. Lauritsen, T. Huus, and S. G. Nilsson, Phys. Rev. **92**, 1501 (1953).
[21] A. Galonsky *et al.*, Phys. Rev. **98**, 586 (1955).
[22] I. Ja. Barit, Ju. G. Balashko, L. S. Dulkova, and V. P. Zavarzina, Sov. J. Nucl. Phys. **29**, 585 (1979).
[23] S. Nagata, S. Yamaguchi, Y. Fujino, Y. Hori, and N. Sugiyama, Nucl. Instrum. Methods B **6**, 533 (1985).
[24] F. Besenbacher, I. Stensgaard, and P. Vase, Nucl. Instrum. Methods B **15**, 459 (1986).
[25] A. J. Kellock and J. E. E. Baglin, Nucl. Instrum. Methods B **79**, 493 (1993).
[26] V. Quillet, F. Abel, and M. Schott, Nucl. Instrum. Methods B **83**, 47 (1993).
[27] G. G. Ohlsen and P. G. Young, Nucl. Phys. **52**, 134 (1964).
[28] M. Bruno, F. Cannata, M. D'Agostino, C. Maroni, and I. Massa, Il Nuovo Cim. **68**, 35 (1982).

[29] R. Ishigami *et al.*, J. Nucl. Sci. Tech. **41**, 953 (2004).
[30] G. Mani and A. Tarratts, Nucl. Phys. A **107**, 624 (1968).
[31] R. A. Hardekopf *et al.*, Nucl. Phys. A **287**, 237 (1977).
[32] L. S. Senhouse and T. A. Tombrello, Nucl. Phys. **57**, 624 (1964).
[33] J. C. Allred, D. K. Froman, A. M. Hudson, and L. Rosen, Phys. Rev. **82**, 786 (1951).
[34] R. G. Freemantle *et al.*, Philos. Mag. **45**, 1090 (1954).
[35] W. T. H. van Oers and K. W. Brockman, Nucl. Phys. **44**, 546 (1963).
[36] T. Kambara, M. Takai, M. Nakamura, and S. Kobayashi, J. Phys. Soc. Jpn. **44**, 704 (1978).
[37] W. Gruebler *et al.*, Nucl. Phys. A **242**, 265 (1975).
[38] E. J. Stephenson, H. E. Conzett, R. M. Larimer, B. T. Leemann, R. Roy, and P. von Rossen, Phys. Rev. C **21**, 44 (1980).
[39] J. M. Blair, G. Freier, E. E. Lampi, and W. Sleator, Phys. Rev. **75**, 1678 (1949).
[40] L. Stewart, J. E. Brolley, and L. Rosen, Phys. Rev. **128**, 707 (1962).
[41] M. Bruno, F. Cannata, M. D'Agostino, C. Maroni, and I. Massa, Lett. Nuovo Cimemto **27**, 265 (1980).
[42] H. Jett, J. J. L. Detch, and N. Jarmie, Phys. Rev. C **3**, 1769 (1971).
[43] L. D. Blokhintsev, V. I. Kukulin, and V. N. Pomerantsev, Phys. At. Nucl. **68**, 1120 (2005).
[44] J. P. Davidson, *Collective Models of the Nucleus* (Academic, New York, 1968).
[45] J. Cederberg, D. Olsen, J. Larson, G. Rakness, K. Jarausch, J. Schmidt, B. Borovsky, P. Larson, and B. Nelson, Phys. Rev. A **57**, 2539 (1998).
[46] L. Canton and L. G. Levchuk, Nucl. Phys. A **808**, 192 (2008).